Nwafor Solomon Chibuzo
PG/MENG/19/91987
Control Engineering
DEPARTMENT OF ELECTRONIC ENGINEERING, UNIVERSITY OF NIGERIA, NSUKKA

Linear State Estimation of an LPV-Quadcopter model with Linear Kalman Filter (LKF)

State Estimation-Kalman Filter

State estimate is vital to the performance of feedback-based control techniques. Consequently, numerous state estimation techniques for quadrotor UAVs have been reported in prior research. These strategies establish input/output-based methods for measuring unknown states as shown in Figure 2.25. Additionally, these methods are frequently employed to troubleshoot defective sensors.

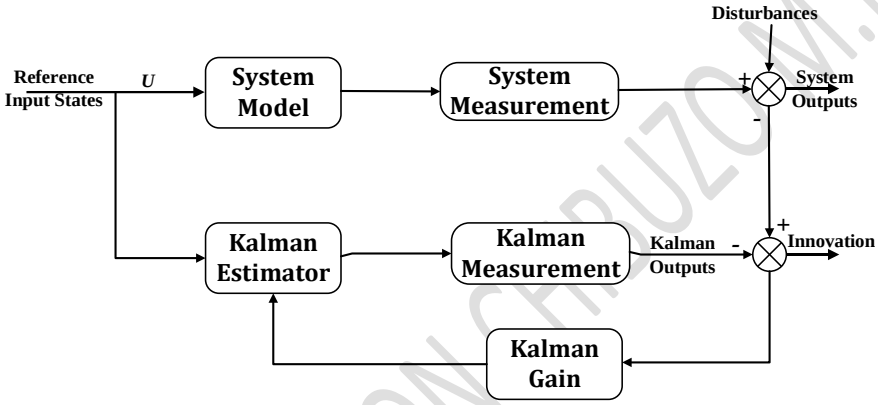

Figure 2.25: Linear Kalman filter

Several approaches to the problem of attitude estimation have been developed over time, and various sensor data fusion algorithms have been built and validated on-board [1]. The most well-known techniques use complementary filters because of their low computing demand [2]. A complementary filter estimates quaternion in the same way as an algebraic solution of a system employing inertial/magnetic measurements does in [3].

The estimate of the posture was addressed in [4] using a Dual Quaternion Multiplicative Extended Kalman Filter (DQ-MEKF). Using dual quaternion multiplication and the idea of error unit dual quaternion, this method is an extension of the Quaternion Multiplicative Extended Kalman Filter, which is commonly applied for spacecraft attitude determination. In [5], Euler angles were used to determine the transformation matrix between the North-East-Down (NED) frame and the body frame. In addition, the Complementary Filter was implemented by determining the Euler angles using the gyroscope, magnetometer, and accelerometer. In [6], a quaternion-based attitude unscented Kalman filter was developed, with quaternion errors parameterized by small-angle approximations and a magnetometer-

only spacecraft scenario in mind. The method was applied to a filter with an attitude quaternion and gyro bias vector as its state vector. [7] was tasked with establishing the optimal filter for a physical object to improve the quadrotor's stability. In order to accomplish this, they devised a study technique with a laboratory station for testing quadrotor drones. Without adjusting the structure of these filters in order to optimize the existing flight controllers, they concentrated on an examination of the most widely used filters for flight stabilization. A low-cost navigation device including an inertial measurement unit (IMU), five ultrasonic range sensors, and an optical flow camera was utilized to implement a Kalman filtering-based sensor fusion system [8]. They are regarded a multi-rate variant of the Extended Kalman Filter to accommodate heterogeneous sensors with variable sampling rates and the existence of nonlinearities in the model. The efficiency of the proposed sensor platform was evaluated using numerical simulations on a quadrotor flying simulator.

UAV Design Model

The UAV is a six degrees of freedom (DoF) system with three (3) DoF as position dimensions (X-axis, Y-axis, Z-axis) and three (3) DoF as orientation dimensions (ϕ-axis, θ-axis, ψ-axis). As shown in Figure 3.2, an x-shape multirotor quadcopter with M1 and M3 revolving clockwise and M2 and M4 rotating counter-clockwise is used. The locations and orientations of the body frame in relation to the inertial frame [9].

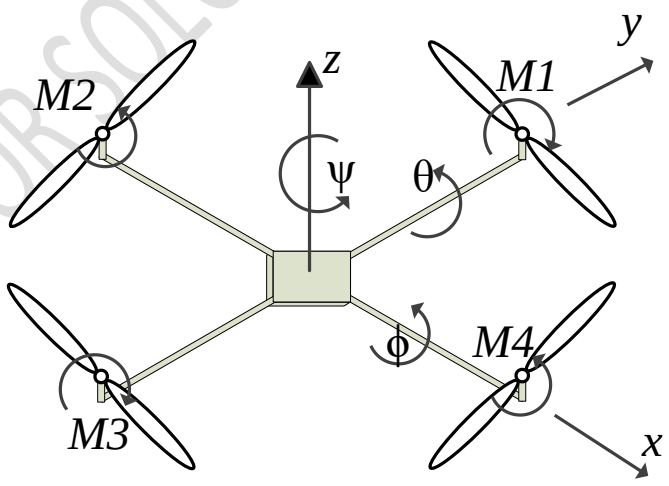

Figure 3.2: X-shaped multirotor quadcopter configuration

3.2.1 UAV Kinematics

Nwafor Solomon Chibuzo
PG/MENG/19/91987
Control Engineering
DEPARTMENT OF ELECTRONIC ENGINEERING, UNIVERSITY OF NIGERIA, NSUKKA

To define the position of the UAV in space, a position vector, $\vec{P}$, which runs from the initial frame origin to the body frame origin is employed, as illustrated in Figure 3.3. The Initial frame's position vector, $\vec{P}$, is provided by (1) as:

$$\vec{P} = [X\ Y\ Z]^T \tag{1}$$

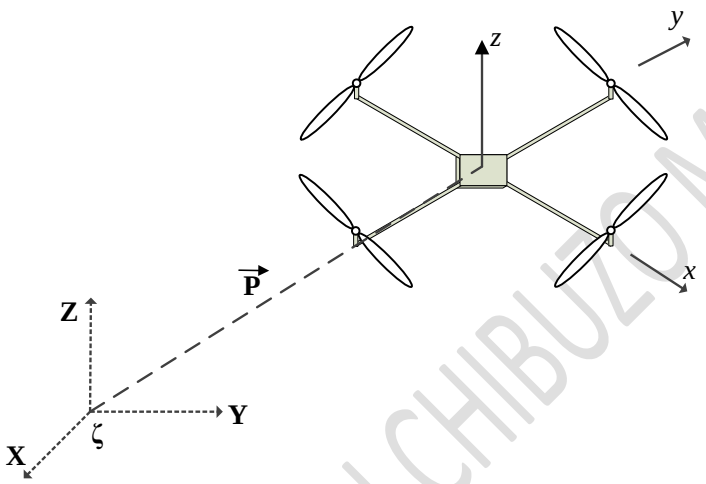

Figure 3.3: UAV position in space

3.2.1.1 Euler Angles

There are twenty-four (24) conventions used to characterize the attitude of a UAV. As illustrated in Figure 3.4, an $\boldsymbol{R_{zyx}}$ convention is adopted for the UAV design. Euler angles were used to complete the body-frame rotation. The rotation was performed in accordance with the right-hand rule.

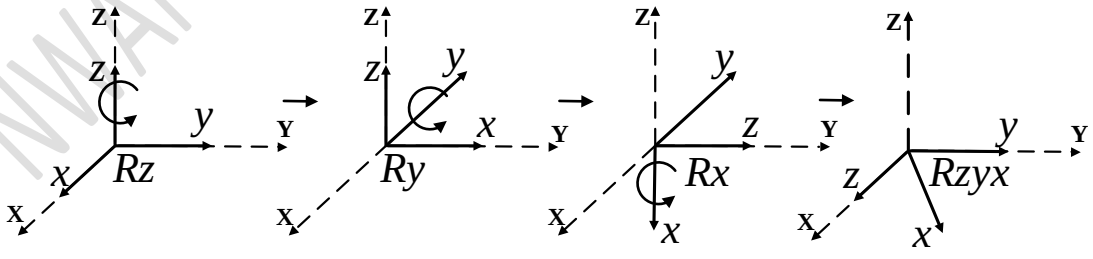

Figure 3.4: Right hand rule rotation of the UAV

Nwafor Solomon Chibuzo
PG/MENG/19/91987
Control Engineering
DEPARTMENT OF ELECTRONIC ENGINEERING, UNIVERSITY OF NIGERIA, NSUKKA

(2), (3), and (4) were obtained by rotating the UAV from Rz to Rx, and we have a product of $\boldsymbol{R_{zyx}}$ as specified in (5) that is valid for both the inertial frame, $\boldsymbol{R_{XYZ}}$, and the body frame, $\boldsymbol{R_{zyx}}$.

$$R_z = \begin{bmatrix} Cos\psi & -Sin\psi & 0 \\ Sin\psi & Cos\psi & 0 \\ 0 & 0 & 1 \end{bmatrix} \tag{2}$$

$$R_y = \begin{bmatrix} Cos\theta & 0 & Sin\theta \\ 0 & 1 & 0 \\ -Sin\theta & 0 & Cos\theta \end{bmatrix} \tag{3}$$

$$R_x = \begin{bmatrix} 1 & 0 & 0 \\ 0 & Cos\phi & -Sin\phi \\ 0 & Sin\phi & Cos\phi \end{bmatrix} \tag{4}$$

$$R_{zyx} = \begin{bmatrix} Cos\psi\text{Cos}\theta & Cos\psi\text{Sin}\theta\text{Sin}\phi - \text{Sin}\phi\text{Sin}\psi & Cos\psi\text{Cos}\phi\text{Sin}\theta + \text{Sin}\phi\text{Sin}\theta \\ Cos\theta\text{Sin}\psi & Sin\psi\text{Sin}\phi\text{Sin}\theta + \text{Cos}\phi\text{Cos}\psi & Sin\psi\text{Sin}\theta\text{Cos}\phi - \text{Cos}\psi\text{Sin}\phi \\ -Sin\theta & Cos\theta\text{Sin}\phi & Cos\phi\text{Cos}\theta \end{bmatrix} \tag{5}$$

Since the body frame is mounted to the UAV, typical UAV velocity measurements were conducted in the body frame. The linear velocities of the body frame cause the unmanned aerial vehicle to translate along the body frame axis. These are the linear velocities:

$$\dot{x}\ \left(v, \frac{m}{s}\right), \dot{y}\ \left(u, \frac{m}{s}\right), and\ \dot{z}\ (w, \frac{m}{s})$$

Consequently, while the UAV travels through space, it experiences both linear and rotational velocities. To control the UAV in space, $\dot{X}\ \dot{Y}\ \dot{Z}$ linear velocities in the Inertial frame were determined. A rotation matrix is utilized to convert the linear velocities in the body frame, $\vec{V}^B$, to the inertial frame employing the Euler angle rotation method as stated in (6).

$$\vec{\dot{P}}^E = R_{zyx}\vec{v}^B_{zyx} \tag{6}$$

Where $\vec{v}^B_{zyx} = [u\ v\ w]^T$ (7)

$$\vec{\dot{P}}^E = \left[\dot{X}\ \dot{Y}\ \dot{Z}\right]^T \tag{8}$$

According to (6), $\vec{v}^B_{zyx}$ is given as:

$$\vec{v}^B_{zyx} = \left(R_{zyx}\right)^1 \vec{\dot{P}}^E \tag{9}$$

For angular velocities, the origin of the body frame remains constant, but the UAV simply spins around the body frame axes. These are the angular velocities p (rad/s), q (rad/s), and r (rad/s). A transfer matrix, T, is created to relate the angular velocities of the body frame to the inertial frame angular velocities ($\dot{\phi},\ \dot{\theta}, \dot{\psi}$) as defined in (10).

$$\overrightarrow{\omega}^B = T(\phi,\theta)^1\vec{\dot{\alpha}} \tag{10}$$

Where $\begin{bmatrix}\vec{\dot{\alpha}} \\ \overrightarrow{\omega}^B\end{bmatrix} = \begin{bmatrix}\dot{\phi}\ \dot{\theta}\ \dot{\psi} \\ \dot{\phi}\ \dot{\theta}\ \dot{\psi}\end{bmatrix}^T$ (11)

$$T(\phi,\theta) = \begin{bmatrix}1 & Sin\phi\tan\theta & Cos\phi\tan\theta \\ 0 & Cos\phi & -Sin\phi \\ 0 & Sin\phi\mathrm{Sec}\theta & Cos\phi\mathrm{Sec}\theta\end{bmatrix} \tag{12}$$

3.2.2 UAV Dynamics

The dynamics of the UAV were constructed using the assumption that the UAV is a rigid body. We considered two types of motions: translational and rotational motions.

3.2.2.1 UAV Translational Motion

Newton's second law of motion is used for a three-degree-of-freedom (DoF) UAV to derive translational motion (X, Y, Z). The control forces and control torque ($U_1\ U_2\ U_3\ U_4$) from Figure 3.5 are applied to the UAV body frame.

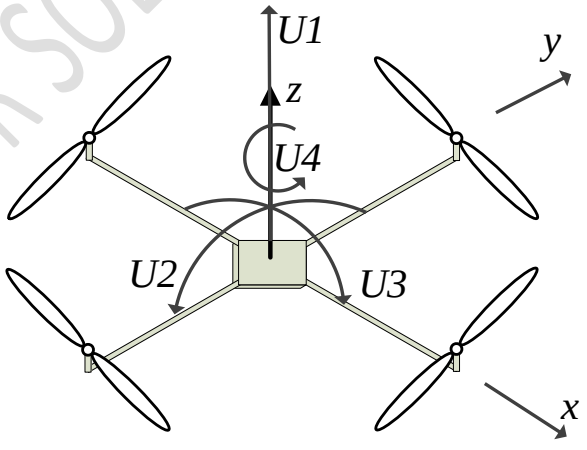

Figure 3.5: The UAV control inputs

The translational equations of motion is derived by calculating the net force, $\vec{F}_{net}^{B}$ on the body frame, which is defined in (13) as:

$$\vec{F}_{net}^{B} = m\vec{v}^{B} \tag{13}$$

According to (6), the velocity vector of the UAV in the body frame is as follows:

$$\vec{v}^{B} = u\hat{\imath} + v\hat{\jmath} + w\hat{k} \tag{14}$$

$\hat{\imath}, \hat{\jmath}, \hat{k}$ are unit vectors representing directions in the body frame; hence, (15) is obtained as the derivative of (14) as follows:

$$\dot{\vec{v}}^{B} = \dot{u}\hat{\imath} + \dot{v}\hat{\jmath} + \dot{w}\hat{k} + u\dot{\hat{\imath}} + v\dot{\hat{\jmath}} + w\dot{\hat{k}} \tag{15}$$

Since the UAV rotates with the body frame, $\dot{\hat{\imath}} = \dot{\hat{\jmath}} = \dot{\hat{k}} \neq 0$; therefore, the unit directions are rotated to obtain the angular velocities with respect to their unit directions, as illustrated in Figure 3.6. This does not impact the position of the UAV.

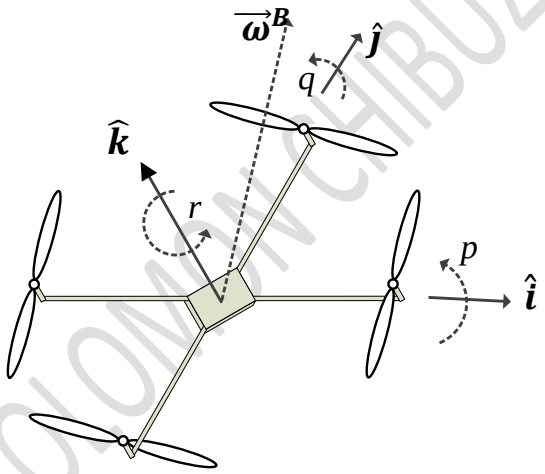

Figure 3.6: UAV unit rotation direction

From Figure 3.6, $\overrightarrow{\omega}^{B}$ is the angular velocity vector in the body frame and is defined as follows in (16):

$$\begin{bmatrix} \dot{\hat{\imath}} \\ \dot{\hat{\jmath}} \\ \dot{\hat{k}} \end{bmatrix} = \begin{bmatrix} \overrightarrow{\omega}^{B} & 0 & 0 \\ 0 & \overrightarrow{\omega}^{B} & 0 \\ 0 & 0 & \overrightarrow{\omega}^{B} \end{bmatrix} \begin{bmatrix} \hat{\imath} \\ \hat{\jmath} \\ \hat{k} \end{bmatrix} \tag{16}$$

We calculated the net force in the body frame by substituting (16) and (15) into (13) as defined in (17).

$$\vec{F}_{net}^{B} = m(\vec{v}_{zyx}^{B} + \vec{\omega}^{B} x\, \vec{v}^{B}) \tag{17}$$

As a result, (17) is the translational motion obtained from Newton's second law, which can be enlarged further in (18) as:

$$\begin{bmatrix} F_x \\ F_y \\ F_z \end{bmatrix}^B = \left[\begin{bmatrix} m & 0 & 0 \\ 0 & m & 0 \\ 0 & 0 & m \end{bmatrix} \begin{bmatrix} \dot{u} \\ \dot{v} \\ \dot{w} \end{bmatrix} + \begin{bmatrix} p \\ q \\ r \end{bmatrix} x \begin{bmatrix} m & 0 & 0 \\ 0 & m & 0 \\ 0 & 0 & m \end{bmatrix} \begin{bmatrix} u \\ v \\ w \end{bmatrix} \right] \quad (18)$$

3.2.2.2 UAV Rotational Motion

The basic equations to characterize the orientation of the UAV in space is obtained by applying Newton's second law to the body frame, as defined in (19).

$$\sum \vec{M}_{ext}^B = \frac{d\vec{h}}{dt} = \frac{(\bar{\bar{I}}\vec{\omega})^B}{dt} \quad (19)$$

Where $\sum \vec{M}_{ext}^B$ = net moment in the body frame,

$\frac{d\vec{h}}{dt}$ = Angular momentum,

And $\bar{\bar{I}}$ = Inertia Tensor = $\begin{bmatrix} I_{xx} & -I_{xy} & -I_{xz} \\ -I_{yx} & I_{yy} & -I_{yz} \\ -I_{zx} & -I_{zy} & I_{zz} \end{bmatrix}$ (20)

All of the products of inertia from (20) are symmetrical along the diagonal of $\bar{\bar{I}}$ and equal to zero because they were measured in the body frame. As a result, (20) can be rewritten as (21).

$$\bar{\bar{I}} = \begin{bmatrix} I_{xx} & 0 & 0 \\ 0 & I_{yy} & 0 \\ 0 & 0 & I_{zz} \end{bmatrix} \quad (21)$$

When (17) and (19) are compared, the net moment in the body frame becomes:

$$\sum \vec{M}_{ext}^B = \bar{\bar{I}}\dot{\vec{\omega}}^B + \vec{\omega}^B \, x \left(\bar{\bar{I}}\vec{\omega}\right)^B \quad (22)$$

The rotating motion of the UAV in body frame is represented by (22) and may be stated in vector form as:

$$\begin{bmatrix} M_x \\ M_y \\ M_z \end{bmatrix} = \left(\begin{bmatrix} I_{xx} & 0 & 0 \\ 0 & I_{yy} & 0 \\ 0 & 0 & I_{zz} \end{bmatrix} \begin{bmatrix} \dot{p} \\ \dot{q} \\ \dot{r} \end{bmatrix} \right) + \begin{bmatrix} p \\ q \\ r \end{bmatrix} x \left(\begin{bmatrix} I_{xx} & 0 & 0 \\ 0 & I_{yy} & 0 \\ 0 & 0 & I_{zz} \end{bmatrix} \begin{bmatrix} p \\ q \\ r \end{bmatrix} \right) \quad (23)$$

(17) and (23) represent our UAV's dynamical behavior in space and were combined in (24) as:

$$\begin{bmatrix} \vec{F}^B \\ \vec{M}^B \end{bmatrix} = \begin{bmatrix} mI_{3x3} & 0_{3x3} \\ 0_{3x3} & \bar{\bar{I}} \end{bmatrix} \begin{bmatrix} \vec{v}^B_{zyx} \\ \vec{\omega}^B \end{bmatrix} + \begin{bmatrix} \vec{\omega}^B x\, \vec{v}^B \\ \vec{\omega}^B\, x\, (\bar{\bar{I}}\vec{\omega})^B \end{bmatrix} \quad (24)$$

3.2.3 UAV Forces and Moments

3.2.3.1 Force Due to Gravity

In the inertial frame, the UAV weight always points opposite the z-axis. We used a rotation matrix as stated in to determine the force due to gravity in the body frame (25).

$$\overrightarrow{W}^B = \left(R_{zyx}\right)^{-1} \overrightarrow{W}^E \quad (25)$$

Where $\overrightarrow{W}^E = [0 \quad 0 \quad -mg]^T$

By substituting (5) for (25), the vectorized force due to gravity is derived as:

$$\overrightarrow{W}^B = \begin{bmatrix} mg.Sin\theta \\ -mg.Cos\theta \text{Sin}\phi \\ -mg.Cos\phi \text{Cos}\theta \end{bmatrix} \quad (26)$$

3.2.3.2 UAV Input Forces

As illustrated in Figure 3.5, a righthand rule of rotation is used to obtain the input forces operating on the UAV, such as thrust acting in the z-direction of the body frame, U1, roll control moment, U2, pitch moment, U3, and yaw moment, U4. In the body frame, the input force vector, $\vec{F}_{IN}$, is defined as follows:

$$\vec{F}_{IN} = [0 \quad 0 \quad U1 \quad U2 \quad U3 \quad U4]^T \quad (27)$$

3.2.3.3 UAV Gyroscopic Effect

The gyroscopic impact of our UAV solely influences the moments in the body frame, as shown in Figure 3.8. The gyroscopic effect on the UAV is calculated and an angular velocity vector of the motors is defined in (28).

$$\vec{\Omega} = \vec{\Omega}_1 - \vec{\Omega}_2 + \vec{\Omega}_3 - \vec{\Omega}_4 \quad (28)$$

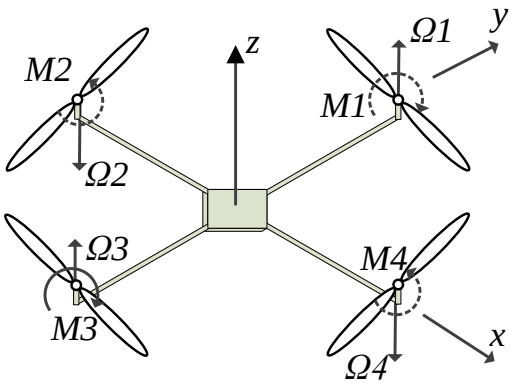

Figure 3.8: UAV moment of inertia

According to Newton's second law, the moments of gyroscopic effect, $\vec{M}_G$, are now as follows:

$$\vec{M}_G = \vec{\omega}^B x \vec{H}^B \quad (29)$$

$\vec{H}^B$ is the angular momentum on the motors from (29), and it is expressed as:

$$\vec{H}^B = J\vec{\Omega} \quad (30)$$

In(30), J represents the mass moment of inertia about the z-axis of the body frame, and(29) can be written in vector form as follows:

$$\vec{M}_G = [0 \quad 0 \quad 0 \quad qJ\Omega \quad -pJ\Omega \quad 0]^T \quad (31)$$

(26),(27), and(31) are summed together to get the total forces and moments operating on the UAV:

$$\vec{\Sigma} = \vec{W}^B + \vec{F}_{IN} + \vec{M}_G \quad (32)$$

3.2.4 UAV State Space Representation

In order to examine the UAV state model further, the UAV is reformulated in state space to maintain track of the derived model from (9) and (10). Furthermore, by equating (24) to (32) and making the greatest order in the equation the subject, (33), (34), and (35) are obtained [9].

$$\begin{bmatrix}\dot{u}\\ \dot{v}\\ \dot{w}\\ \dot{p}\\ \dot{q}\\ \dot{r}\end{bmatrix}=\begin{bmatrix}g & 0 & 0 & 0 & 0 & 0\\ 0 & -g & 0 & 0 & 0 & 0\\ 0 & 0 & -g & 0 & 0 & 0\\ 0 & 0 & 0 & 0 & 0 & 0\\ 0 & 0 & 0 & 0 & 0 & 0\\ 0 & 0 & 0 & 0 & 0 & 0\end{bmatrix}\begin{bmatrix}Sin\theta\\ Cos\theta\text{Sin}\phi\\ Cos\theta\text{Cos}\phi\\ 0\\ 0\\ 0\end{bmatrix}+\begin{bmatrix}0 & r & 0 & 0 & -w & 0\\ -r & 0 & 0 & w & 0 & 0\\ q & 0 & 0 & -u & 0 & 0\\ 0 & 0 & 0 & 0 & s & t.q\\ 0 & 0 & 0 & -k & 0 & l.p\\ 0 & 0 & 0 & d.q & 0 & 0\end{bmatrix}\begin{bmatrix}u\\ v\\ w\\ p\\ q\\ r\end{bmatrix}+$$

$$\begin{bmatrix}0 & 0 & 0 & 0 & 0 & 0\\ 0 & 0 & 0 & 0 & 0 & 0\\ 0 & 0 & 1/m & 0 & 0 & 0\\ 0 & 0 & 0 & 1/I_{xx} & 0 & 0\\ 0 & 0 & 0 & 0 & 1/I_{yy} & 0\\ 0 & 0 & 0 & 0 & 0 & 1/I_{zz}\end{bmatrix}\begin{bmatrix}0\\ 0\\ U1\\ U2\\ U3\\ U4\end{bmatrix} \quad (33)$$

$$\begin{bmatrix}\dot{X}\\ \dot{Y}\\ \dot{Z}\end{bmatrix}=R_{zyx}\begin{bmatrix}u\\ v\\ w\end{bmatrix} \quad (34)$$

$$\begin{bmatrix}\dot{\phi}\\ \dot{\theta}\\ \dot{\psi}\end{bmatrix}=T(\phi,\theta)\begin{bmatrix}p\\ q\\ r\end{bmatrix} \quad (35)$$

Where s = $\frac{J}{I_{xx}}$, $t = = \frac{(I_{yy}-I_{zz})}{I_{xx}}$, $k = \frac{J}{I_{yy}}$, $l = \frac{(I_{zz}-I_{xx})}{I_{yy}}$, $d = \frac{(I_{xx}-I_{yy})}{I_{zz}}$

3.2.5 Runge-Kutta Integration Approach

An advanced integrator known as the Runge-kutta fourth-order approach is employed to integrate the state space into new state variables for the controllers. Twelve state variables from both the body frame and the inertial frame are obtained using this integrator. It is assumed that the UAV's current states $(u_k, v_k, w_k, p_k, q_k, r_k, X_k, Y_k, Z_k, \theta_k, \phi_k, \psi_k)$ were known. Runge Kutta states that [9]:

$$\vec{X}_{k+1} = \vec{X}_k + \vec{X}_{k,w}.T_s \quad (36)$$

From (36), $\vec{X}_{k+1}$ *is the new state vectors* $\left(\vec{v}^B_{k+1}, \vec{P}^E_{k+1}, and\ \vec{\theta}^E_{k+1}\right)$*to be calculted*

$\vec{X}_k$ *is the known current state vectorswhich are;*

$$\vec{v}^B_k = [u_k\ v_k\ w_k\ p_k\ q_k\ r_k]^T$$

$$\vec{P}^E_k = [X_k\ Y_k\ Z_k]^T$$

$$\vec{\theta}^E_k = [\theta_k\ \phi_k\ \psi_k]^T$$

$\vec{X}_{k,w}$ *is the weighted average slope expressed as* $\frac{1}{6}(\dot{x}_{k1} + 2\dot{x}_{k2} + 2\dot{x}_{k3} + \dot{x}_{k4})$

T_s *is the sample time.*

The new UAV integrated states are computed as:

$$\begin{bmatrix} u_{k+1} \\ v_{k+1} \\ w_{k+1} \\ p_{k+1} \\ q_{k+1} \\ r_{k+1} \\ X_{k+1} \\ Y_{k+1} \\ Z_{k+1} \\ \theta_{k+1} \\ \phi_{k+1} \\ \psi_{k+1} \end{bmatrix} = \begin{bmatrix} 1 & 0 & 0 & 0 & 0 & 0 & 0 & 0 & 0 & 0 & 0 & 0 \\ 0 & 1 & 0 & 0 & 0 & 0 & 0 & 0 & 0 & 0 & 0 & 0 \\ 0 & 0 & 1 & 0 & 0 & 0 & 0 & 0 & 0 & 0 & 0 & 0 \\ 0 & 0 & 0 & 1 & 0 & 0 & 0 & 0 & 0 & 0 & 0 & 0 \\ 0 & 0 & 0 & 0 & 1 & 0 & 0 & 0 & 0 & 0 & 0 & 0 \\ 0 & 0 & 0 & 0 & 0 & 1 & 0 & 0 & 0 & 0 & 0 & 0 \\ 0 & 0 & 0 & 0 & 0 & 0 & 1 & 0 & 0 & 0 & 0 & 0 \\ 0 & 0 & 0 & 0 & 0 & 0 & 0 & 1 & 0 & 0 & 0 & 0 \\ 0 & 0 & 0 & 0 & 0 & 0 & 0 & 0 & 1 & 0 & 0 & 0 \\ 0 & 0 & 0 & 0 & 0 & 0 & 0 & 0 & 0 & 1 & 0 & 0 \\ 0 & 0 & 0 & 0 & 0 & 0 & 0 & 0 & 0 & 0 & 1 & 0 \\ 0 & 0 & 0 & 0 & 0 & 0 & 0 & 0 & 0 & 0 & 0 & 1 \end{bmatrix} \begin{bmatrix} u_k \\ v_k \\ w_k \\ p_k \\ q_k \\ r_k \\ X_k \\ Y_k \\ Z_k \\ \theta_k \\ \phi_k \\ \psi_k \end{bmatrix} + \begin{bmatrix} \dot{u}_{k,w} \\ \dot{v}_{k,w} \\ \dot{w}_{k,w} \\ \dot{p}_{k,w} \\ \dot{q}_{k,w} \\ \dot{r}_{k,w} \\ \dot{X}_{k,w} \\ \dot{Y}_{k,w} \\ \dot{Z}_{k,w} \\ \dot{\theta}_{k,w} \\ \dot{\phi}_{k,w} \\ \dot{\psi}_{k,w} \end{bmatrix} T_s \quad (37)$$

3.2.6 UAV Control Inputs and Rotor Angular Velocities

A relationship between the control inputs and rotor angular velocities of the UAV is established.

3.2.6.1 UAV Compressible Airflow

According to the ISA design considerations, Bernoulli's equation for compressible airflow is used to calculate the calibrated airspeed, V_c, for subsonic flow as described in (38).

$$V_c = \sqrt{\frac{2a_0^2}{\gamma - 1}\left[\left(\frac{P_T - P_S}{P_0} + 1\right)^{\frac{\gamma-1}{\gamma}} - 1\right]} \quad (38)$$

where P_T *is the total air pressure*

P_S *is the static air pressure*

P_0 *is atmospheric pressure* $(101325.0\ \mathrm{P}a)$

a_0 *is the speed of sound*

γ *is the heat capacity ratio*

Nwafor Solomon Chibuzo
PG/MENG/19/91987
Control Engineering
DEPARTMENT OF ELECTRONIC ENGINEERING, UNIVERSITY OF NIGERIA, NSUKKA

3.2.6.2 Aerodynamics of the UAV

The calibrated airspeed from Bernoulli's equation (38) is employed as the rotor speed for the UAV. Figure 3.9 illustrates a top view of the UAV rotor rotating clockwise with an angular rotation rate of *Ω(rad/s)*. The rotor blade has a total length of *R (m)*, an airfoil of *dr(m)*, a length from the blade's center to its tip of *r(m)*, and rotates at a speed of *ΩR (m/s)*.

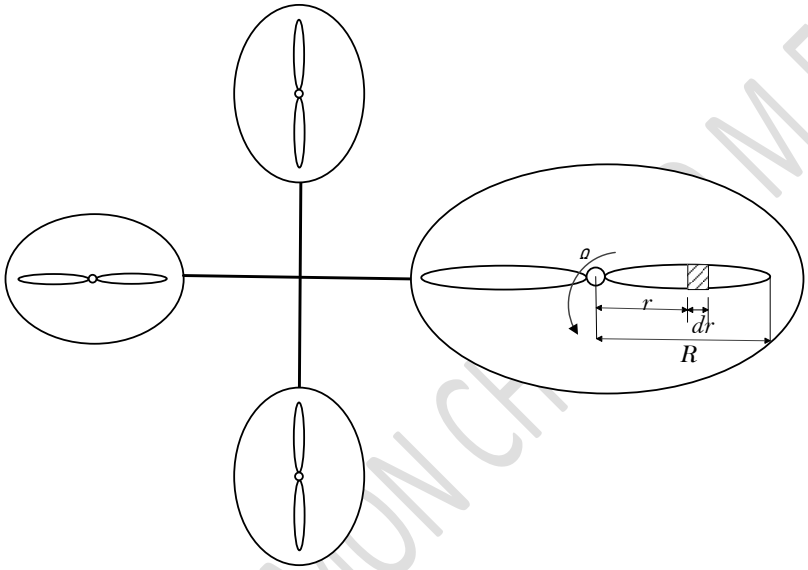

Figure 3.9: Top view of the UAV rotor

Aerodynamics is utilized to calculate the thrust of the UAV, *T* and the thrust difference, dT is determined as:

$$dT = dL - dD\phi \tag{39}$$

dL denotes the differential lift force, [N], and dD denotes the differential drag force, [N], as stated in (40) and (41).

$$dL = C_L \frac{1}{2} \rho . {V_c}^2 . c . dr \tag{40}$$

$$dD = C_D \frac{1}{2} \rho . {V_c}^2 . c . dr \tag{41}$$

Where $C_L = coefficient\ of\ lift$

$C_D = coefficient\ of\ drag$

$\rho = air\ density. we\ adopted\ the\ ISA\ \rho_0$

$c = cord\ length$

$dr = differential\ width\ of\ the\ airfoil$

$V_c =$

$Resultant\ air\ velocity\ which\ is\ the\ same\ as\ the\ callibrated\ air\ speed\ in\ Eqtn$

The air velocity vector is resolved using Pythagoras theorem as shown in Figure 3.10 as

$$V_c = \sqrt{\Omega.r^2 + Va^2} \tag{42}$$

From (42), $\Omega.r\ is\ the\ Airfoil\ velocity$

$Va\ is\ the\ velocity\ formed\ by\ blade\ with\ air$. This velocity is negligible because $\Omega.r \gg Va$.

Therefore (42) becomes,

$$V_c = \Omega.r \tag{43}$$

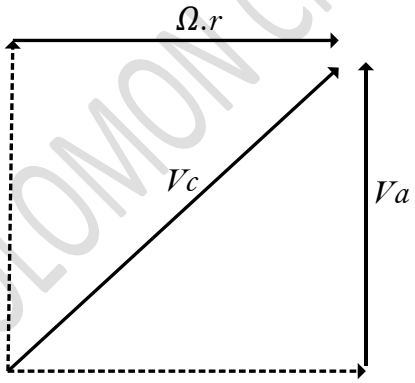

Figure 3.10: UAV resultant air velocity vector

For a complete blade, (40) and (41) are substituted into (39) and the integral was taken with respect to r to get the UAV thrust as defined in (44).

$$T = \Omega^2.\rho.\int_0^R c[C_L - C_D\phi]\, r^2 dr \tag{44}$$

From (44), $\rho.\int_0^R c[C_L - C_D\phi]\, r^2 dr = C_T$

Where $C_T = Thrust\ factor$.

Therefore,

$$T = \Omega^2 . C_T \tag{45}$$

From (45), we computed the UAV control inputs (*U1, U2, U3, and U4*) as:

$$\begin{bmatrix} U1 \\ U2 \\ U3 \\ U4 \end{bmatrix} = \begin{bmatrix} C_T & C_T & C_T & C_T \\ 0 & L.C_T & 0 & -L.C_T \\ -L.C_T & 0 & L.C_T & 0 \\ -C_Q & C_Q & -C_Q & C_Q \end{bmatrix} \begin{bmatrix} \Omega_1^2 \\ \Omega_2^2 \\ \Omega_3^2 \\ \Omega_4^2 \end{bmatrix} \tag{46}$$

Where *L is the distance from center of the UAV frame*

C_Q = Torque factor, (-1) C_T.

Recall that (47a) provides the UAV's total angular velocity, and from (46), a relationship between the control inputs and the angular velocities is established as defined in (47), and expanded in (48), (49), (50), and (51) respectively.

$$\Omega = \Omega_1 + \Omega_2 + \Omega_3 + \Omega_4 \tag{47}$$

$$\Omega_1 = \left(\frac{1}{4}\frac{U_1}{C_T} - \frac{1}{2}\frac{U_3}{C_T} . L - \frac{1}{4}\frac{U_4}{C_Q} \right)^{1/2} \tag{48}$$

$$\Omega_2 = \left(\frac{1}{4}\frac{U_1}{C_T} + \frac{1}{2}\frac{U_2}{C_T} . L + \frac{1}{4}\frac{U_4}{C_Q} \right)^{1/2} \tag{49}$$

$$\Omega_3 = \left(\frac{1}{4}\frac{U_1}{C_T} + \frac{1}{2}\frac{U_3}{C_T} . L - \frac{1}{4}\frac{U_4}{C_Q} \right)^{1/2} \tag{50}$$

$$\Omega_4 = \left(\frac{1}{4}\frac{U_1}{C_T} - \frac{1}{2}\frac{U_2}{C_T} . L + \frac{1}{4}\frac{U_4}{C_Q} \right)^{1/2} \tag{51}$$

3.3 UAV State Estimation

Figure 3.11 shows how the state of the UAV is estimated using an advanced state estimator known as the linear Kalman filter (LKF). The discrete UAV model is given an input control vector, $\vec{u}_k$, and uncorrelated Gaussian white noise. The new state is measured using noise as an output of the UAV model and compared to the Kalman output measurement at the innovation.

Nwafor Solomon Chibuzo
PG/MENG/19/91987
Control Engineering
DEPARTMENT OF ELECTRONIC ENGINEERING, UNIVERSITY OF NIGERIA, NSUKKA

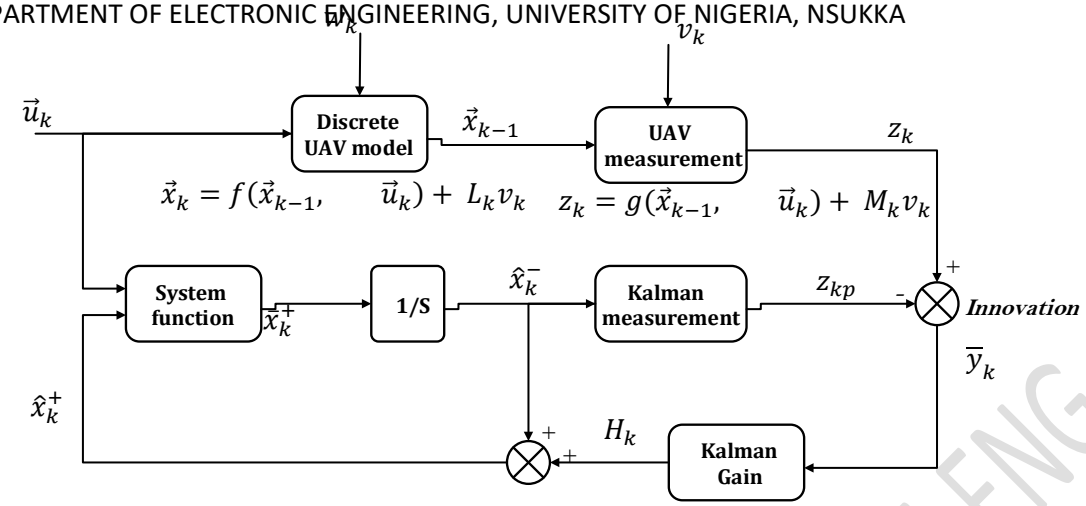

Figure 3.11: UAV Kalman filter state estimation

The aimed of LKF is to estimate the position and velocity of the UAV in space using remote observations. The position of the UAV is specified as a unidimensional random motion model. Because the UAV lacks onboard sensors, the filter will not have information about the UAV's status during tracking. To overcome this problem, it is assumed that the UAV input is noisy rather than deterministic. As the UAV input, Gaussian noise with non-stationary states is used. In (52) and (53) the process is defined to be estimated in a three-dimensional discrete time instance. The UAV model is reformulated into a linear parameter varying (LPV) structure in order to employ the linear Kalman filter model defined in (54). LPV is a linear representation of the UAV's nonlinearities.

$$x_i = A_i \vec{x}_{k-1} + L_i w_k \quad (52)$$

$$x_k = A_k \vec{x}_{k-1} + L w_k \quad (53)$$

$$z_k = H_k \vec{x}_{k-1} + M v_k \quad (54)$$

Where A_i = State transition matrix

$A_k = I + A_i . Ts$ (LPV State transition matrix)

$I \; and \; Ts$= Identity matrix and sample time respectively

$\vec{x}_{k-1}$ = State vector of the system

L_i= Noise input matrix

$L = L_i \; x \; Ts$ (LPV Noise input matrix)

H_k = Measurement model matrix

M = Measurement model noise sensitivity matrix

$w_k \; and \; v_k$ = Uncorrelated Gaussian white noise

z_k = Measurement output vector of the positions given as $\left[P_{xl} \; P_{yl} \; P_{za}\right]^T$ where P_{xl} is the latitude, P_{yl} is the longitude and P_{za} is the altitude.

(53) and (54) were expressed in vector-matrix form, as defined in (55) and (56), respectively.

$$\begin{bmatrix} P_x \\ P_y \\ P_z \\ V_x \\ V_y \\ V_z \end{bmatrix} = \begin{bmatrix} 1 & 0 & 0 & \Delta t & 0 & 0 \\ 0 & 1 & 0 & 0 & \Delta t & 0 \\ 0 & 0 & 1 & 0 & 0 & \Delta t \\ 0 & 0 & 0 & 1 & 0 & 0 \\ 0 & 0 & 0 & 0 & 1 & 0 \\ 0 & 0 & 0 & 0 & 0 & 1 \end{bmatrix} \begin{bmatrix} P_{x-1} \\ P_{y-1} \\ P_{z-1} \\ V_{x-1} \\ V_{y-1} \\ V_{z-1} \end{bmatrix}_k + \begin{bmatrix} \frac{1}{2}\Delta t^2 & 0 & 0 \\ 0 & \frac{1}{2}\Delta t^2 & 0 \\ 0 & 0 & \frac{1}{2}\Delta t^2 \\ \Delta t & 0 & 0 \\ 0 & \Delta t & 0 \\ 0 & 0 & \Delta t \end{bmatrix} \begin{bmatrix} a_x \\ a_y \\ a_z \end{bmatrix} \tag{55}$$

$$\begin{bmatrix} P_{xL} \\ P_{yL} \\ P_{za} \end{bmatrix} = \begin{bmatrix} 1 & 0 & 0 & 0 & 0 & 0 \\ 0 & 1 & 0 & 0 & 0 & 0 \\ 0 & 0 & 1 & 0 & 0 & 0 \end{bmatrix} \begin{bmatrix} P_{x-1} \\ P_{y-1} \\ P_{z-1} \\ V_{x-1} \\ V_{y-1} \\ V_{z-1} \end{bmatrix}_k + Mv_k \tag{56}$$

A set of random variables, σ_a, for the uncorrelated noises $w_k \; and \; v_k$, is created and assumed a normal distribution of zero matrix of Q and R as specified in (57) and (58).

$$w_k \approx N(0, Q) \tag{57}$$

Where $Q = \begin{bmatrix} \sigma_{ax}^2 & 0 & 0 \\ 0 & \sigma_{ay}^2 & 0 \\ 0 & 0 & \sigma_{az}^2 \end{bmatrix}$

$$v_k \approx N(0, R) \tag{58}$$

Where $R = \begin{bmatrix} \sigma_{ax}^2 & 0 & 0 \\ 0 & \sigma_{ay}^2 & 0 \\ 0 & 0 & \sigma_{az}^2 \end{bmatrix}$

An optimal recursive data processing technique that has two processes is used

3.3.1 Kalman Filter Prediction Step

This step uses a previous estimate to generate an actual estimate as described in (59) and (60).

$$\overline{x}_k^+ = A_k \hat{x}_k^+ + L w_k \tag{59}$$

$$P_k^- = A_k P_{k-1}^+ A_k^T + LQL^T \tag{60}$$

Where $\overline{x}_k^+$ = a priori state estimate

P_k^- = a priori covariance estimate

For a valid distribution in LQL^T, $\sigma_a = \sigma_{ax} = \sigma_{ay} = \sigma_{az}$ such that (57) will now become:

$$w_k \approx L.N(0, \sigma_a^2)$$

And $LQL^T = \sigma_a^2 \begin{bmatrix} \frac{1}{2}\Delta t^2 & 0 & 0 & & 0_{3x3} & \\ 0 & \frac{1}{2}\Delta t^2 & 0 & \Delta t & 0 & 0 \\ 0 & 0 & \frac{1}{2}\Delta t^2 & 0 & \Delta t & 0 \\ & 0_{3x3} & & 0 & 0 & \Delta t \end{bmatrix}$

3.3.2 Kalman Filter Update Step

The update step combines the estimation from the prediction step with the actual measurement to enhance the estimated state. The state of the UAV will be updated based on the amount of the innovation, $\bar{y}_k$, using the Kalman filter gain, K_k, which is produced as a ratio between the innovation uncertainty and the current state uncertainty as defined in (61).

$$\hat{x}_k^+ = \hat{x}_k^- + K_k \bar{y}_k \tag{61}$$

Where $\hat{x}_k^-$ = Previous state estimate without the measurement information

$\hat{x}_k^+$ = Current state estimate updated by Kalman gain and Innovation.

The Kalman gain matrix quantifies state uncertainty, P_{k-1}^- weighted as a ratio of measurement uncertainty as defined in (62).

$$K_k = P_{k-1}^- H_k^T S_k^{-1} \tag{62}$$

Where $P_{k-1}^- = Uncertianty\ of\ the\ state$

S_k^{-1} = Uncertainty of the innovation covarience which covariance is defined in (63).

$$S_k = H_k P_{k-1}^{-} H_k^T + R_k \tag{63}$$

$\bar{y}_k$ is the error between measurement, z_k and the predicted measurement, z_{kp} as defined in (64)

$$\bar{y}_k = z_k - z_{kp} \tag{64}$$

Where $z_{kp} = H_k \hat{x}_k^{-}$

To reduce uncertainty and enhance accuracy, the covariance of the state estimate must be adjusted as defined in (65).

$$P_k^{+} = (I - K_k H_k) P_{k-1}^{-} \tag{65}$$

References

[1] Ahmed, H.; Tahir, M. Accurate attitude estimation of a moving land vehicle using low-cost MEMS IMU sensors. *IEEE Trans. Intell. Transp. Syst.* 2016, *18*, 1723–1739. [CrossRef]

[2] Wu, J.; Zhou, Z.; Fourati, H.; Li, R.; Liu, M. Generalized linear quaternion complementary filter for attitude estimation from multisensor observations: An optimization approach. *IEEE Trans. Autom. Sci. Eng.* 2019, *16*, 1330–1343. [CrossRef]

[3] Valenti, R.G.; Dryanovski, I.; Xiao, J. Keeping a good attitude: A quaternion-based orientation filter for IMUs and MARGs. *Sensors* 2015, *15*, 19302–19330. [CrossRef]

[4] Filipe, N., Kontitsis, M., and Tsiotras, P. (2015). Extended Kalman Filter for Spacecraft Pose Estimation Using Dual Quaternions. *Journal of Guidance, Control, and Dynamics*, 38(9), 1–17. doi:10.2514/1.G000977.

[5] Huang, Y.h., Rizal, Y., and Ho, M.t. (2015). Development of Attitude and Heading Reference Systems. 13 18.

[6] Challa, M.S., Moore, J.A.Y.G., and Rogers, D.J. (2016). A Simple Attitude Unscented Kalman Filter: Theory and Evaluation in a Magnetometer-Only Spacecraft Scenario. 1845–1858.

[7] Salwa M, Krzysztofik I. Application of Filters to Improve Flight Stability of Rotary Unmanned Aerial Objects. Sensors (Basel). 2022 Feb 21;22(4):1677. doi: 10.3390/s22041677. PMID: 35214577; PMCID: PMC8875604.

[8] Bassolillo SR, D'Amato E, Notaro I, Ariante G, Del Core G, Mattei M. Enhanced Attitude and Altitude Estimation for Indoor Autonomous UAVs. *Drones*. 2022; 6(1):18. https://doi.org/10.3390/drones6010018

[9] M. Misin, V. Puig. LPV MPC Control of an Autonomous Aerial Vehicle. *28th Mediterranean Conference on Control and Automation (MED)*, 2020; 109-114. http://dx.doi.org/10.1109/MED48518.2020.9183041